NJC

ROYAL SOCIETY OF CHEMISTRY

PAPER

View Article Online
View Journal | View Issue

Cite this: *New J. Chem.*, 2020, **44**, 5884

Sustainable production of pyruvic acid: oxidative dehydrogenation of lactic acid over the FeMoO/P catalyst†

Chunyu Yin,[a] Xinli Li,*[a] Zhi Chen,[a] Weixin Zou,[b] Yanli Peng,[a] Song Wei,[a] Congming Tang *[a] and Lin Dong [b]

Fe–Mo bimetallic oxide catalysts doped with elemental P (FeMoO/P) were synthesized using a hydrothermal method, followed by calcination in air. The resultant catalysts were used to catalyze the oxidative dehydrogenation of lactic acid to pyruvic acid using air as an oxidant. UV-Vis characterization revealed that Fe_2O_3 was highly dispersed on the surface of MoO_3 for the FeMoO/P sample due to the enhanced band gap energy. The FeMoO/P sample showed distinct diffraction lines of MoO_3, while the diffraction of the typical (011) line slightly shifted to a higher 2 theta value. This indicated the incorporation of Fe^{3+} into the MoO_3 lattice, forming a surface substituted Fe–O_x–Mo solid solution. Furthermore, the other characterization techniques such as XPS and H_2-TPR disclosed a strong interaction between Fe_2O_3 and MoO_3 by binding energy shift and reducible peak change, respectively. The enhanced oxidizability of Fe species is responsible for the activation of the α-OH group in the lactic acid molecule, transferring hydrogen to the adjacent FeO_x site to achieve a crucial step for the oxidative dehydrogenation of lactic acid. For comparison, the Fe–Mo bimetallic oxide catalyst offered far better activity than its corresponding monometallic oxide/physically mixed oxide due to the increasing oxidizability of FeMoO/P by electron transfer between Fe and Mo species. On-line analysis of the tail gas revealed that no hydrogen was detected, precluding direct dehydrogenation of lactic acid to form pyruvic acid during the catalytic reaction. Furthermore, the experimental results in the absence of O_2, replaced by N_2, showed that a small amount of pyruvic acid formed, and it gradually decreased with time on stream, demonstrating lattice oxygen as an active species for the oxidative dehydrogenation of lactic acid. Encouragingly, the oxidative dehydrogenation reaction of lactic acid over the FeMoO/P catalyst proceeded efficiently at around 60 h on stream and with an excellent selectivity (>70%).

Received 8th January 2020,
Accepted 9th March 2020

DOI: 10.1039/d0nj00118j

rsc.li/njc

Introduction

Obtaining chemicals and fuels from biomass and its derivatives has attracted a great interest in recent years since the concept of sustainable development is widely accepted all over the world.[1–4] Lactic acid (LA) has been produced on a large scale for several decades by using biological maize fermentation technology. Currently, glycerol,[5–10] sugars,[11] and cellulose[12] are also used to synthesize LA by chemical catalysis consisting of oxidation/hydrolysis reactions. Undoubtedly, these technologies provide an excellent basis for the catalytic conversion of LA into other chemicals, such as acrylic acid,[13,14] propionic acid,[15,16] pyruvic acid (PA),[17,18] poly-lactic acid, 2,3-pentanedione,[19] acetaldehyde,[20] and lactates. Among these lactic acid derived chemicals, PA is widely used in the production of food spices, food additives, amino acids, antioxidants and chemical intermediates.[17,21]

A traditional industrial approach for the production of PA includes the dehydration and decarboxylation of tartaric acid with a stoichiometric amount of $KHSO_4$, consuming high energy.[17] In contrast, oxidative dehydrogenation of LA to PA *via* heterogeneous catalysis is viewed as a potential route, which has been reported by several research groups.[17,18] However, a serious challenge exists for this route since both LA and PA have high reactivity during the catalytic reaction, resulting in parallel side reactions and tandem side reactions. Thus, developing highly selective catalysts and optimizing reaction parameters are still desirable.

Oxidative dehydrogenation of LA to PA usually includes liquid and vapor approaches. For the former, the major superiority

[a] *School of Chemistry and Chemical Engineering, Chongqing University of Technology, Chongqing 400054, P. R. China. E-mail: lixinli@cqut.edu.cn, tcmtang2001@163.com*
[b] *Jiangsu Key Laboratory of Vehicle Emissions Control, Center of Modern Analysis, Nanjing University, Nanjing 210093, P. R. China*

† Electronic supplementary information (ESI) available. See DOI: 10.1039/d0nj00118j

is a low reaction temperature (*ca.* <100 °C), which can suppress a great number of side reactions, achieving a high selectivity toward PA.[17,22,23] The weakness is that the catalytic reaction occurs in alkaline media, such as NaOH or LiOH, leading to the formation of pyruvates. To obtain PA, it is necessary to treat pyruvates with inorganic acids through acidification reactions, leading to generation of a large number of waste salts. Compared with the former, the latter only requires one step for achieving PA through the direct transformation of LA, avoiding stoichiometric consumption of base and acid.[18,24–26] However, the major weakness is the high reaction temperature (*ca.* >190 °C) and relatively low selectivity to PA.

In contrast, vapor phase oxidative dehydrogenation of LA to PA does not consume stoichiometric base and acid, making it a benign environmental process. Thus, for nearly two decades, much work has focused on this topic. The early work reported that different structural iron phosphates offered a different activity for the oxidative dehydrogenation of LA to PA, and the M phase consisting of both Fe^{2+} and Fe^{3+} ions displayed the best performance with LA conversion of 60% and PA selectivity of 62%.[25,27] Subsequently, in the same research group, modified iron phosphates having a small amount of Pd/Mo were developed, and the activity was further improved.[28,29] Recently, bimetallic oxides, such as Nb–Ni–O[26] and Mo–Ti–O,[18] have also been further developed to improve activity for the oxidative dehydrogenation of LA using their tunable oxidative-reducibility. Besides, trimetallic oxides, such as Mo–V–Nb, have also been investigated for this reaction by Mao and co-workers.[24] However, both relatively low PA selectivity and deficiency in stability of the catalyst are observed due to the high reactivity of both LA and PA molecules. A possible way for improving the catalytic performance in this reaction required disclosure of the co-effect between redox and acidic–basic properties during the catalytic reactions. However, knowledge on this topic is still quite limited so far. Therefore, a persistent effort for improving the catalytic performance in the oxidative dehydrogenation of LA to PA has to go on.

In the present work, we constructed P doped Fe–Mo bimetallic oxide catalysts for the oxidative dehydrogenation of LA to PA using the hydrothermal synthesis method. Furthermore, the cooperative effect between acidic–basic properties and the redox properties of the catalyst on the oxidative dehydrogenation of LA has been deeply discussed to develop highly efficient catalysts.

Results and discussion

Characterization

BET analysis. Measuring the textural property of a heterogeneous catalyst is an important step to understand the area-specific catalytic rate and mass transfer of reactants and products.[30,31] In this section, the specific surface area, pore volume and pore distribution of the catalysts were investigated using nitrogen adsorption–desorption at 77 K using a JW-BK100C instrument, and the results are depicted in Table 1 and Fig. S1 (ESI†). From the BET data given in Table 1, the single metal oxides, such as FeO and MoO, have lower specific surface areas, 15.2 $m^2\ g^{-1}$ and 9.7 $m^2\ g^{-1}$, respectively.

Table 1 Textural properties of samples

Samples	S_{BET} ($m^2\ g^{-1}$)	V_P ($cm^3\ g^{-1}$)	Pore diameter[a] (nm)
FeO	15.2	0.11	12.4
MoO	9.7	0.05	8.8
FeMoO/P	23.7	0.12	13.7
FeMoO/P*	21.8	0.19	18.1

[a] Calculated from the desorption branch data using the Barrett–Joyner–Halenda (BJH) model.

However, their bimetallic oxide (FeMoO/P, 23.7 $m^2\ g^{-1}$) and the mixture (FeMoO/P*, 21.8 $m^2\ g^{-1}$) show obviously increased specific surface areas. Similarly, the pore volume and pore size of FeMoO/P and FeMoO/P* also increased when compared with their corresponding single metal oxides.

XRD and FT-IR analysis. The structures of the samples were characterized with a wide angle X-ray diffraction (XRD) instrument and a Fourier transform infrared (FT-IR) spectrometer, and the results are shown in Fig. 1 and Table 2. From the XRD patterns depicted in Fig. 1a, FeO presents three characteristic diffraction peaks at $2\theta = 33.3^\circ$, 35.8° and 54.3°, respectively, which agreed well with Fe_2O_3, with the corresponding faces (104), (110) and (116). MoO presents three characteristic diffraction peaks at $2\theta = 23.1^\circ$,

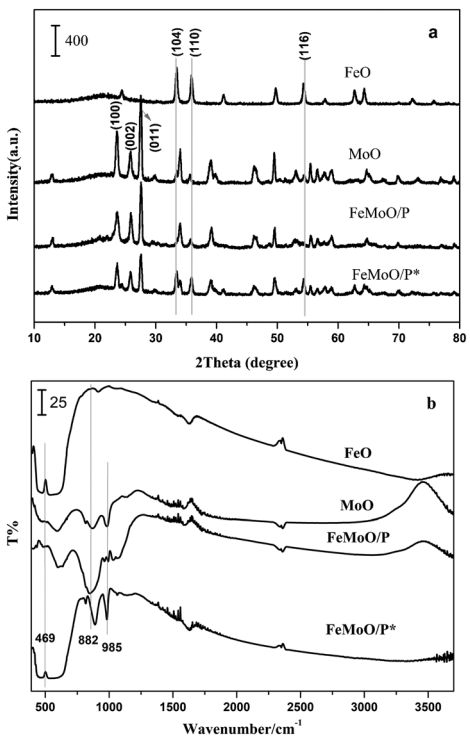

Fig. 1 XRD patterns (a) of fresh samples before reaction and their corresponding FT-IR spectra (b).

Table 2 Structural properties of samples

	MoO(011) plane		
Sample	2θ (°)	d (nm)	Crystalline size (nm)
MoO	27.53	0.3237	22.08
FeMoO/P	27.56	0.3234	21.34

25.8° and 27.4°, respectively, which agreed well with MoO_3, with the corresponding faces, (100), (002) and (011). FeMoO/P was prepared using the hydrothermal method, followed by calcination in air, and it almost remained consistent with the sample of MoO in terms of the diffraction peaks, whereas the characteristic diffraction peaks ascribed to Fe_2O_3 were hardly observed. Furthermore, the diffraction of the typical (011) line indexed to MoO_3 slightly shifted to a higher 2 theta value (see Table 2). This indicated the incorporation of Fe^{3+} into the MoO_3 lattice, forming a surface substituted Fe–O_x–Mo solid solution.[32] The result can be supported by the characterization data of XPS since the Fe/Mo atomic ratio obtained from XPS is 11 : 9, higher than the 1 : 2 ratio of the raw materials. In addition, FeMoO/P had almost the same size as MoO, suggesting a highly dispersed nature of FeO species on the surface of MoO_3. As for the sample of FeMoO/P*, it showed respective characteristic diffraction peaks ascribed to both MoO and FeO samples, meaning a mechanical mixing. FT-IR spectra in the fingerprint region (400–1300 cm^{-1}) can be used to differentiate the structure of samples with slight variations. A difference in characteristic absorption bands at 469, 882, and 985 cm^{-1} was observed by comparing the four samples, which suggested a strong interaction between MoO and FeO in FeMoO/P (shown in Fig. 1b).

UV-Vis, XPS and H_2-TPR analysis. In order to further understand the interaction between MoO and FeO in FeMoO/P, UV-Vis absorption spectra were obtained. According to a recent report,[18] the enhanced band gap energy can be utilized to characterize the dispersion of some metallic oxides. We recorded the UV-Vis spectra and derived Tauc plots, depicted in Fig. S2a and b (ESI†), respectively. Pure FeO and FeMoO/P* have almost the same band gap of 2.0 eV, agreeing well with that reported by Liu *et al.*[33] For the FeMoO/P sample, the band gap is drastically shifted to a higher energy of 2.8 eV, further confirming the higher dispersion of FeO species. The interaction between MoO and FeO in the FeMoO/P sample can also be investigated by XPS measurement, and the results are shown in Fig. 2. Indeed, the binding energy of Fe $2p_{3/2}$ in FeMoO/P was shifted from 710.98 eV (FeO) to 711.69 eV, an increase of 0.71 eV (Fig. 2a). At the same time, the binding energy of Mo $3d_{5/2}$ in FeMoO/P was shifted from 233.58 eV (sample MoO) to 232.85 eV, a decrease of 0.73 eV (Fig. 2b). The evident electron transfer between FeO and MoO demonstrated the existence of strong interaction, and also indicated a variation of redox properties, which is possibly favorable for the oxidative dehydrogenation of LA to PA during the catalytic conversion of LA. The XPS survey spectra also demonstrated the existence of the P element with a binding energy of 133.5 eV in the three samples of MoO, FeMoO/P and FeMoO/P* (Fig. 2c). Next, H_2-TPR experiments were performed to further study the redox properties, and the results are depicted in Fig. 3. In the four samples, pure FeO displayed the lowest reduction peak, centered at 385 °C, and pure MoO displayed reducible peaks at high temperatures, *ca.* >550 °C. However, the low temperature reducible peak ascribed to the FeO species in the prepared sample FeMoO/P shifted toward high temperatures such as 529 °C, higher than that in the FeMoO/P* sample (439 °C), also indicating a strong interaction in the Fe–O_x–Mo solid solution, which resulted in a variation of redox properties. From these results, it is clear that the enhanced oxidizability of Fe species is favorable for the activation of the α-OH group in the lactic acid molecule, transferring hydrogen to the adjacent FeOx site (see the succedent reaction mechanism).

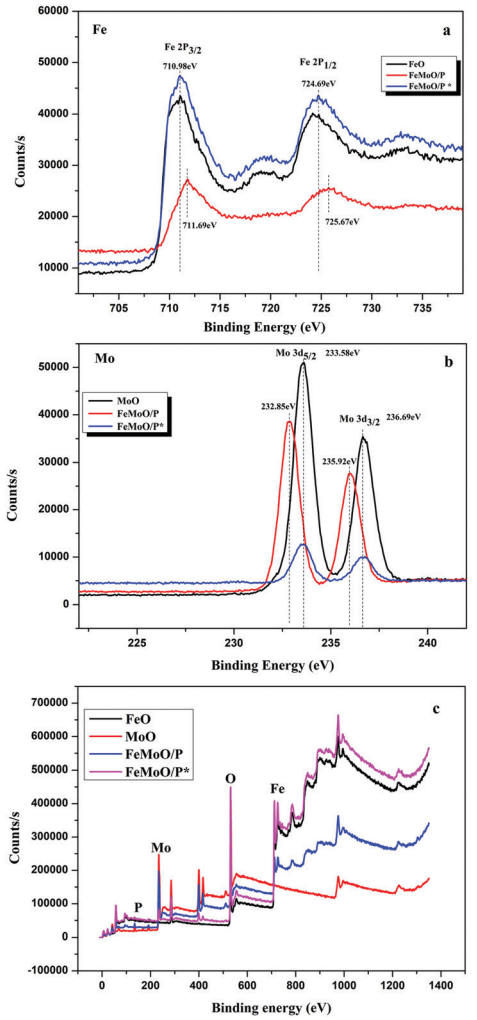

Fig. 2 XPS spectra of fresh samples before reaction (a, Fe 2p; b, Mo 3d; c, survey of all elements).

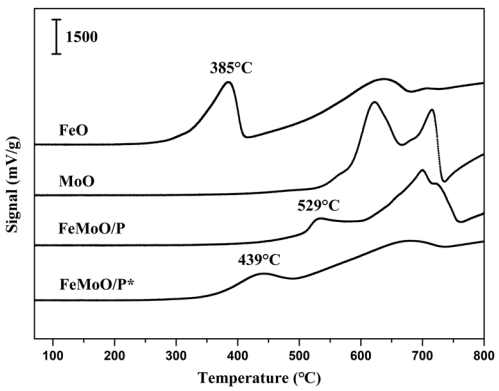

Fig. 3 H_2-TPR profiles of fresh samples before reaction.

Table 3 Conversion of isopropanol

Cat.	Isopropanol conv. (%)	Sel. (%) Propylene	Acetone
FeO	40.4	97.4	2.6
MoO	45.3	96.1	3.9
FeMoO/P	50.8	92.2	7.8
FeMoO/P*	48.9	93.1	6.9

Acidic–basic properties. It is known that surface acidic–basic properties of catalysts play an important role during the catalytic conversion of LA. For example, weak–medium acidity is favorable for the dehydration of LA to acrylic acid,[34–36] and medium acidity is favorable for the decarbonylation of LA to acetaldehyde.[20,37] Stronger acidity tended to accelerate LA polymerization, resulting in the formation of various cokes. Basicity is favorable for LA condensation to 2,3-pentanedione.[19,38–40] Thus, determining the acidity–basicity of the catalyst is necessary for the conversion of LA. As NH_3/CO_2-TPD is the usual means for measuring acidity–basicity, it was naturally first used in this work. The results are shown in Fig. S3 (ESI†). NH_3/CO_2-TPD signals are very weak for all samples, suggesting that the technique struggled to characterize the very weak acidity–basicity of samples. Subsequently, we chose isopropanol as a probe molecule to continuously explore the surface acidity–basicity of samples at 240 °C, which determines acidity according to the obtained product of propylene, and basicity according to the obtained product of acetone.[41] We chose isopropanol as a probe molecule since it has three carbon atoms and one alcoholic hydroxyl group similar to the lactic acid molecule. Especially, the reactive site is focused on the alcoholic hydroxyl group. Table 3 shows the conversion of isopropanol at 240 °C. From the results shown in Table 3, the conversion of isopropanol on all samples is less than 50% at a low feed flow rate of isopropanol (0.5 g h^{-1}), suggesting weak acidic–basic properties on the surface of the catalysts, agreeing well with the results measured by NH_3/CO_2-TPD. It was further found from the distribution of products such as propylene and acetone that acidic sites dominated when compared with the basic sites. Besides, basic sites on FeMoO/P are more numerous than on the others. The basicity of the catalyst is favorable for the first step of esterification between –COOH of the LA molecule and the P–OH group of the catalyst, protecting the –COOH group during the catalytic reaction, to efficiently prohibit the LA decarbonylation reaction to form acetaldehyde; while acidity of the catalyst is favorable for the step of hydrolysis of the pyruvate intermediate to form pyruvic acid.

Catalyst evaluation

Effect of mass transfer during the catalytic reaction. In order to understand the authentic performance of the prepared catalysts,[42,43] preliminary experiments on the internal diffusion limitation and the external diffusion limitation were carried out, and the results are shown in Fig. 4 and 5. From Fig. 4a, the effect of catalyst particle size on the oxidative dehydrogenation of LA to PA was clearly observed, *i.e.*, LA conversion increased drastically with the decrease of the catalyst particle size, suggesting an internal

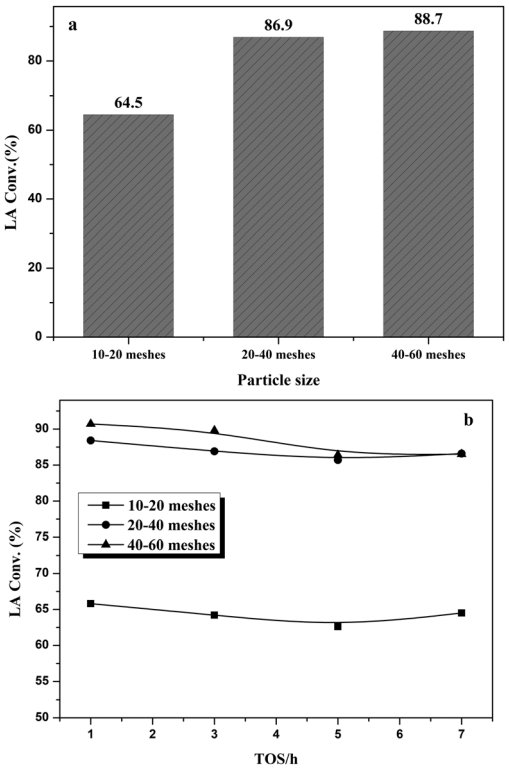

Fig. 4 Effect of catalyst particle size on the oxidative dehydrogenation of LA. Catalyst: FeMoO/P, 0.38 mL, 0.38–0.50 g; reaction temperature, 230 °C; carrier gas air, 3.0 mL min^{-1}; feed flow rate, 2.0 g h^{-1}, LA feedstock, LA 10 wt% in water; TOS, 1–7 h; LA, lactic acid.

diffusion limitation. As the catalyst reduced to 20–40 mesh in particle size, LA conversion is comparable to that in 40–60 mesh, indicating that the internal diffusion limitation can be easily removed. Fig. 4b shows that LA conversion was stable with time on stream, and no induction period occurred for this reaction. Next, 20–40 mesh sizes of the catalyst were used to further investigate the external diffusion limitation. At a fixed LA/O_2 molar ratio and contact time, LA conversion was obviously influenced by LA flow rate (Fig. 5a), suggesting the occurrence of an external diffusion limitation. As the LA flow rate increased to 1.0 mL h^{-1} loading in a 1.5 cm height of the catalyst, the external diffusion limitation was efficiently removed. Similarly, LA conversion was also stable with time on stream (Fig. 5b). In the subsequent experiments for activity evaluation, catalyst particle size was chosen as 20–40 mesh, and LA flow rate was chosen as 2.0 mL h^{-1} loading in a 3.0 cm height of the catalyst in a fixed bed reactor to eliminate the mass transfer effect.

Comparison of catalysts. According to the discussion on mass transfer during the catalytic oxidative dehydrogenation reaction of LA, catalyst particle sizes of 20–40 mesh as well as the LA flow rate of 2 mL h^{-1} were used to evaluate the catalytic performances of samples, which fully excluded the effect of mass transfer. The performances of the four samples in the oxidative dehydrogenation of LA are shown in Table 4 and Fig. 6. For LA conversion, the increased order for these samples is: FeO < MoO ~ FeMoO/P* < FeMoO/P. The difference between the lowest

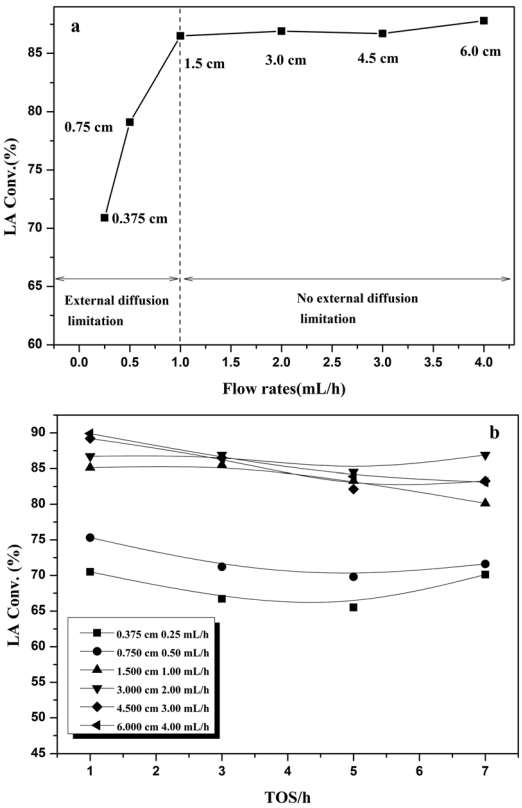

Fig. 5 Effect of LA flow rate on the oxidative dehydrogenation of LA. Catalyst: FeMoO/P, 0.05–1.0 g; reaction temperature, 230 °C; particle size, 20–40 meshes; carrier gas air, 3.0 mL min^{-1}; feed flow rate, 2.0 g h^{-1}, LA feedstock, LA 10 wt% in water; TOS, 1–7 h; LA, lactic acid.

Table 4 Comparison of catalysts in the oxidative dehydrogenation of LA[a]

Catalyst	LA conv. (%)	Sel.[b] (%) PA	AD	AA	Others	LA consumption rate × 10^{-4} mmol (m^2 h)$^{-1}$	PA formation rate × 10^{-4} mmol (m^2 h)$^{-1}$
FeO	58.3	44.3	7.0	15.7	33.0	1.58	0.70
MoO	73.7	21.2	8.3	0.5	70.0	4.49	0.95
FeMoO/P	88.4	74.2	6.9	7.1	11.8	2.91	2.16
FeMoO/P*	71.9	66.1	8.5	1.7	23.7	1.27	0.84

[a] Catalyst, 0.38 mL; reaction temperature, 230 °C; particle size, 20–40 meshes; air, 3.0 mL min^{-1}; feed flow rate, 2.0 mL h^{-1}; LA feedstock, LA 10 wt% in water; TOS, 1–7 h. [b] LA, lactic acid; PA, pyruvic acid; AD, acetaldehyde; AA, acrylic acid.

LA conversion of FeO (58.3%) and the highest LA conversion of FeMoO/P (88.4%) is up to 30.1%. However, the tendency of PA selectivity of these samples does not follow LA conversion, and the new increased order of PA selectivity is: MoO < FeO < FeMoO/P* < FeMoO/P. Similar to LA conversion, the bigger difference value of 53% between the lowest PA selectivity of MoO (21.2%) and the highest PA selectivity of FeMoO/P (74.2%) is observed. These results clearly demonstrate that the oxidative dehydrogenation of LA to PA is a catalytic reaction under the conditions of 230 °C and air as an oxidant, and is sensitive to the catalysts. In addition, the area-specific catalytic rate for the formation of PA (2.16×10^{-4} mmol (m^2 h)$^{-1}$) on FeMoO/P is two times higher than the others.

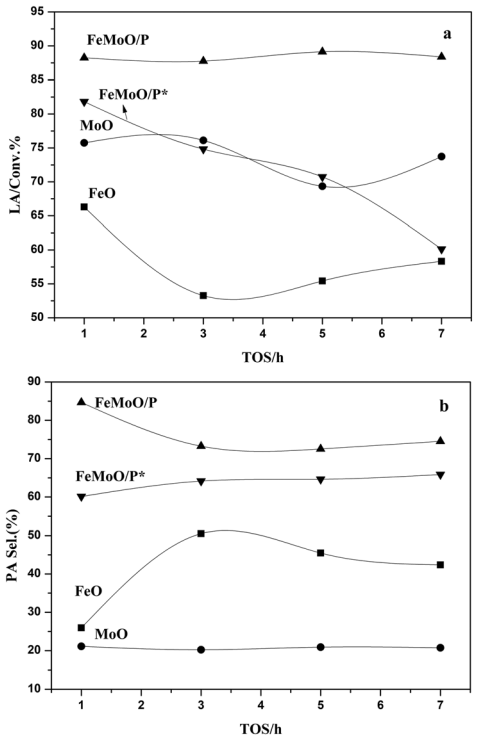

Fig. 6 Time course for LA conversion (a) and PA selectivity (b). Reaction conditions are the same as those in Table 4.

Further understanding of the relationship between the structure, the constituents and the surface property of the catalysts and their activity is an important way to improve catalytic performances during the catalytic oxidative dehydrogenation of LA.[17] Firstly, MoO was evaluated for its activity in the catalytic oxidative dehydrogenation of LA at 200 °C by the Pidko and Hensen group, and it achieved a PA yield of <10%.[18] We enhanced the reaction temperature from 200 °C to 230 °C, and achieved a slightly higher PA yield of 15.6%. In general, a low PA yield necessitated us to add other contents into MoO, and we constructed composite catalysts to improve catalytic performance. In the conversion of LA, Fe based catalysts have been investigated in our previous work,[44] and we found that acidic–basic properties and redox properties were incorporated. For example, in the absence of oxygen, Fe based catalysts displayed acidity for LA decarbonylation to acetaldehyde at low temperature (~300 °C),[44] and redox properties for LA deoxygenation to propionic acid at high temperature (~390 °C).[45,46] Furthermore, we checked the activity of pure FeO in the presence of oxygen, and achieved a better PA yield of 25.8% than MoO. Therefore, we introduced a versatile Fe element into MoO, and constructed composite catalysts. As expected, the composite catalyst of FeMoO/P exhibited excellent performance compared to MoO and FeO alone. From the textural properties of the catalysts shown in Table 1, FeMoO/P has a greater pore size and pore volume than the single metal oxides, lowering the mass transfer resistance of reactants and products, which favors the catalytic reaction of oxidative dehydrogenation of LA.

The constituent elements of catalysts were detected by XPS spectra (Fig. 3c), and the detected elements in FeMoO/P were

Fe, Mo, O and P, respectively. XRD characterization confirmed the incorporation of Fe^{3+} into the MoO_3 lattice to form a surface substituted Fe–O_x–Mo solid solution for FeMoO/P. Electron transfer between Fe and Mo verified by XPS characterization (Fig. 2a and b) efficiently regulates the redox properties of the catalysts, which has been demonstrated by H_2-TPR experiments (Fig. 3). The reduction peak of Fe species shifts from the low temperature of 385 °C to the higher temperature of 529 °C, suggesting that the reducibility decreases, and the oxidizability increases indirectly. Besides, the oxygen content of FeMoO/P is evidently higher than that of the single metal oxides (shown in Table S1, ESI†). Thus, FeMoO/P offered excellent activity, ascribed to an increase of oxidizability. In addition, FeMoO/P displays relatively higher isopropanol conversion, suggesting a higher density of acidic–basic sites compared with other samples. Surface basicity of catalysts favors adsorption and esterification of LA molecules during the oxidative dehydrogenation of LA to PA in the presence of oxygen, whereas surface acidity favors the hydrolysis of the absorbed pyruvate intermediate from the surface of the catalyst to form pyruvic acid. Therefore, appropriate redox and acidic–basic properties are the main factor for improving the oxidative dehydrogenation of LA to PA.

Ratio of LA/O_2. In the preliminary experiment, we replaced oxygen with nitrogen (purity: 99.999 wt%) as the reaction atmosphere, and tested the catalytic performance for the oxidative dehydrogenation of LA to PA, and the results are shown in Fig. 7a and b. At the initial reaction time, LA conversion reached nearly 90%, and quite a bit of PA was formed. For example, PA concentration reached 2.1 wt% in the aqueous solution. With further lengthening of reaction time, LA conversion as well as PA formation rate drastically decreased, suggesting that the catalyst deactivated rapidly. Meanwhile, tail gas analysis confirmed no occurrence of hydrogen, demonstrating that PA was not formed by direct dehydrogenation of LA (Fig. 7c). The used catalysts with different times on stream were characterized by XRD measurements, as shown in Fig. 7d. Characteristic diffraction peaks indexed to oxides decreased rapidly, and then disappeared, whereas the used catalysts, which ran for 7 h on stream under the air atmosphere, remained similar to the fresh sample in characteristic diffraction peaks. Moreover, we also found that the sample running under a N_2 atmosphere restored its initial structure when it was placed under an air atmosphere (Fig. 7e). These results suggested that lattice oxygen can be used for the oxidative dehydrogenation of LA, accompanying the departure of the H_2O molecule. Also, gas phase O_2 in air was adsorbed on the surface of the catalyst, and transformed into lattice oxygen.

Oxygen has been found to play an important role in the oxidative dehydrogenation of LA from the discussion on the preliminary experiments. Further study on the effect of the ratio of LA/O_2 during the catalytic oxidative dehydrogenation of LA is a way to improve catalytic performance. Fig. 8 plots LA conversion and PA selectivity as a function of the ratio of LA/O_2 at 5 h on stream. LA conversion as well as PA selectivity with time on stream at different molar ratios of LA/O_2 is shown in Fig. S4 (ESI†). It was clearly observed that LA conversion continuously increased with a decrease of LA/O_2 molar

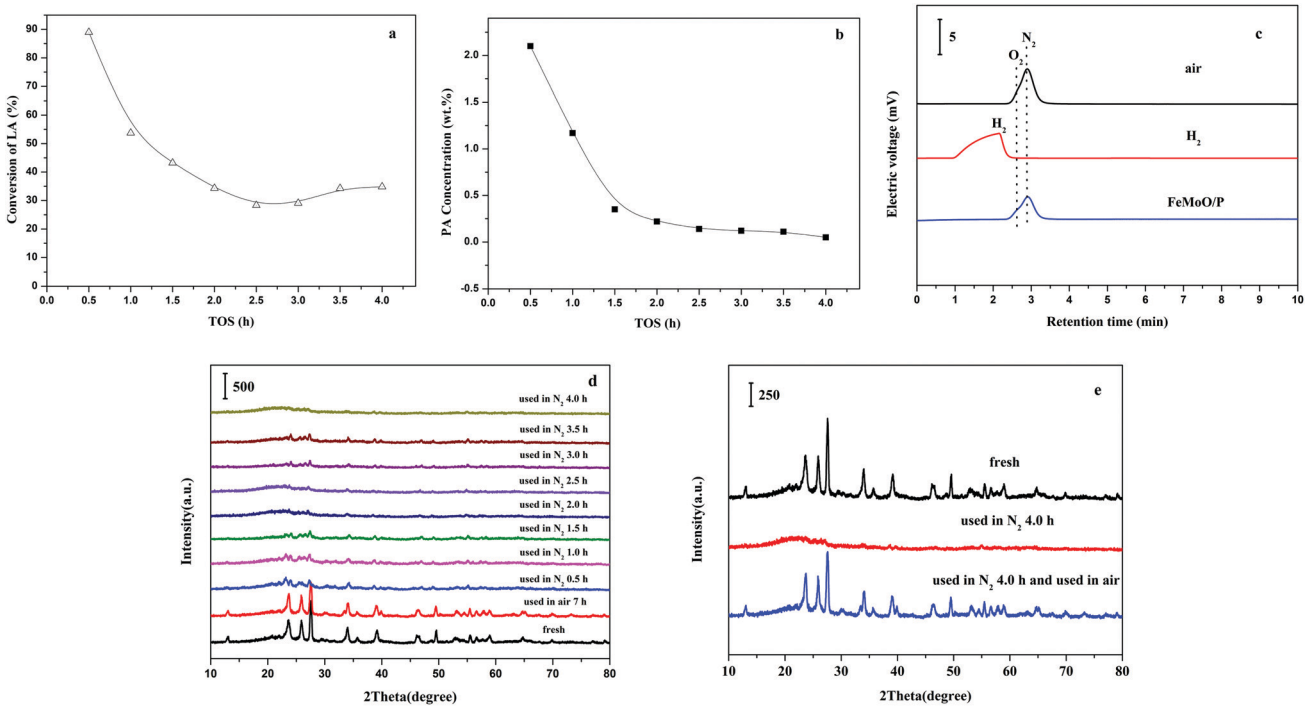

Fig. 7 Performance of the FeMoO/P catalyst: (a) PA concentration with time on stream, (b) LA conversion with time on stream, (c) GC profiles of the tail gas over the FeMoO/P catalyst, compared with reference air and pure hydrogen and (d) XRD patterns. Conditions: reaction temperature, 230 °C; particle size, 20–40 meshes; carrier gas N_2 or air, 3.0 mL min^{-1}; feed flow rate, 2.0 mL h^{-1}; LA feedstock, LA 10 wt% in water; LA, lactic acid; PA, pyruvic acid. (e) XRD patterns of the FeMoO/P catalyst, compared for that used in N_2 for 4.0 h and that used in N_2 for 4.0 h and that used in air.

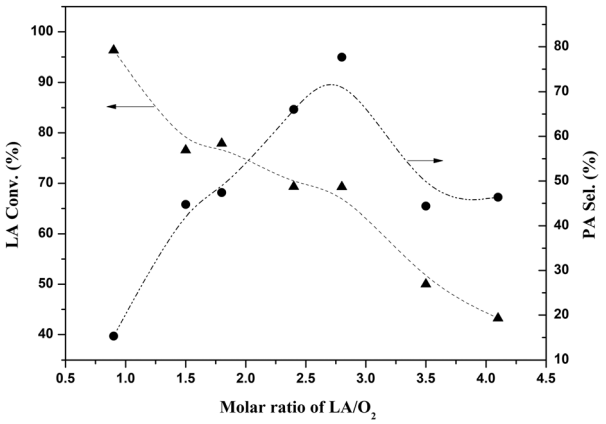

Fig. 8 Effect of LA/O_2 molar ratios. Conditions: catalyst, FeMoO/P, 0.38 mL, 0.37 g; reaction temperature, 230 °C; particle size, 20–40 meshes; carrier gas air, 3.0 mL min^{-1}; feed flow rate, 2.0 mL h^{-1}; LA feedstock, LA 10 wt% in water; TOS, 5 h; LA, lactic acid; PA, pyruvic acid.

ratio. As previously mentioned, oxygen is necessary for the oxidative dehydrogenation of LA since it is required to compensate for losing lattice oxygen. Indeed, at the initial stage of increasing O_2/LA molar ratio, PA selectivity drastically increased. However, PA selectivity decreased with a further increase of O_2/LA molar ratio. In other words, a high concentration of oxygen, *i.e.*, a high O_2/LA molar ratio, caused a worse selectivity toward PA. The reasons can be ascribed to three aspects. First, an appropriate amount of O vacancies, which has been confirmed according to the recent work[32] using O1s XPS spectra, as shown in Fig. 9, favors Fe^{3+} for activating α-OH of the lactic acid molecule. But, high O_2/LA molar ratios decreased O vacancies, resulting in a low formation rate of PA. Further, the parallel side reactions have a high reaction rate at high O_2/LA molar ratios, and it is known that the decarbonylation/decarboxylation of LA to acetaldehyde is a major parallel side reaction during the catalytic conversion of LA.[14,47,48] For example, a larger amount of acetaldehyde was generated at high O_2/LA molar ratios. Secondly, serial reactions increased their reaction rate due to the occurrence of full oxygen and unstable pyruvic acid molecules. In the end, competitive adsorption between LA and the oxygen molecule on the catalyst surface resulted in the decrease of the adsorbed LA molecules, which is not favorable for the conversion of LA to PA *via* oxidative dehydrogenation. Therefore, determining an appropriate O_2/LA molar ratio is very important for improving PA selectivity, and the optimal molar ratio of LA/O_2 is around 2.25–2.75.

Productivity of the FeMoO/P catalyst. The contact time was changed between 0.15 s (corresponding LA flow rate of 4 mL h^{-1}) and 1.2 s (corresponding LA flow rate of 0.5 mL h^{-1}) at the fixed LA/O_2 molar ratio at 230 °C so that the maximum PA productivity was determined for the FeMoO/P sample. The results are depicted in Fig. 10. Clearly, LA conversion increased with lengthening contact time. In contrast, PA productivity decreased. The maximum PA productivity of ~3.5 mmol g^{-1} h^{-1} was achieved for contact times lower than 0.2 s and LA conversion was in the range of 48–60%. Combining the high LA conversion and PA productivity, optimal conditions can be set as a contact time of 0.3 s (the corresponding LA flow rate of 2.0 mL h^{-1} and air flow rate of 3.0 mL min^{-1}), where LA conversion reached 88.4%, and PA productivity reached 3.0 mmol g^{-1} h^{-1}.

Stability. Stability testing is very important for heterogeneous catalyst research from a perspective of industrial application.[49,50] The stability experiment of FeMoO/P was performed in the case of controlling the initial LA conversion at less than 70% in order to achieve fuller saturation of active sites of the catalyst by reactant molecules, and observe a genuine stability (Fig. 11). Controlling low LA conversion has two paths: (1) adopting high LA LHSV (liquid hourly space velocity) and (2) decreasing catalyst usage. Here, we chose the latter. The catalyst was reduced to 30%, and diluted with inert quartz sand. From the data shown in Fig. 11, we can clearly observe that LA conversion remains at 60% and PA selectivity almost remains constant (>70%) at the reaction time of 60 h on stream although LA conversion abruptly decreased near 10% from ~70% to ~60% at the initial reaction time of 10 h. So far, it is a pity that much of the work on the oxidative dehydrogenation of LA has lacked a disclosure of catalyst stability. Fortunately, bare phosphate iron and when it

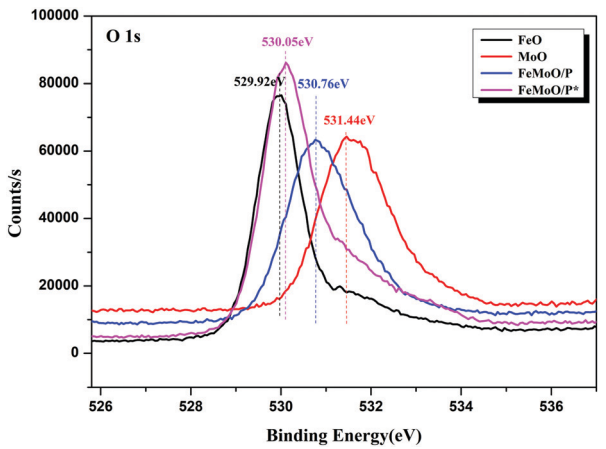

Fig. 9 XPS spectra of O1s in fresh samples before reaction.

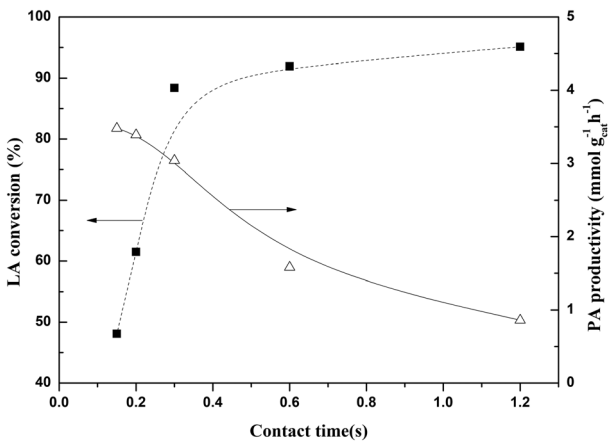

Fig. 10 LA conversion and catalyst productivity for PA as a function of contact time. Conditions: catalyst, FeMoO/P, 0.38 mL, 0.37 g; reaction temperature, 230 °C; particle size, 20–40 meshes; LA feedstock, LA 10 wt% in water. LA, lactic acid; PA, pyruvic acid.

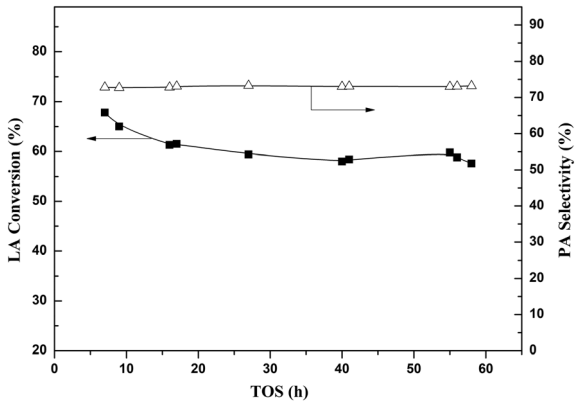

Fig. 11 Stability of the FeMoO/P catalyst. Conditions: catalyst, 0.12 g FeMoO/P and 0.30 g quartz sand, 0.38 mL; reaction temperature, 230 °C; particle size, 20–40 meshes; air, 3.0 mL min^{-1}; feed flow rate, 2.0 mL h^{-1}; LA feedstock, LA 10 wt% in water; LA, lactic acid; PA, pyruvic acid.

is doped with 0.8 wt% Pd catalysts have shown stability for only 10 h on stream due to the presence of Ai, where LA conversion was controlled at ~50% in the initial reaction time, and PA selectivity was observed at ~70%.[28] For bare phosphate iron, LA conversion also decreased by around 10% within the reaction time of 10 h, and longer reaction times were not studied. Comparatively speaking, the stability of the FeMoO/P catalyst for 60 h on stream is a desirable result.

Reaction mechanism. Further investigation of the reaction mechanism for the oxidative dehydrogenation of LA to PA can help to optimize catalyst design and reaction parameters, achieving better catalytic performances. (1) Differentiating the oxygen source: is gas phase oxygen or lattice oxygen utilized during the catalytic oxidative dehydrogenation of LA? On the FeMoO/P catalyst, when nitrogen (N_2) replaces air as a reaction atmosphere, PA is formed, with a decrease in PA forming rate with time on stream, indicating that lattice oxygen is consumed upon the oxidative dehydrogenation of LA to PA (shown in Fig. 12). With further consumption of lattice oxygen in the catalyst, PA formation rate drastically reduces, and LA conversion also quickly decreases. When TOS arrives at 4 h, PA is hardly detected in the liquid samples. Then, when nitrogen is substituted by air as a reaction atmosphere, LA conversion drastically increases, and PA concentration in the liquid sample also increases drastically, indicating that a large amount of PA is formed in the presence of oxygen. At this moment, lattice oxygen can be confirmed as having a role in the oxidative dehydrogenation of LA. Whether gas phase oxygen is directly used in the oxidative dehydrogenation of LA or it is first transformed to lattice oxygen the oxidative dehydrogenation of LA is not confirmed yet. Another experiment in which inert quartz sand was substituted for the catalyst in the presence of air was carried out. As a result, only a trace of PA was detected (see in Table S2, ESI†), demonstrating that gas phase oxygen was not directly used, but it was transformed into lattice oxygen to be used subsequently in the oxidative dehydrogenation of LA.

A catalytic cycle of LA converted to PA over the FeMoO/P catalyst is depicted in Scheme 1. First, LA is combined with the surface of the catalyst *via* an acid–base reaction, in which the

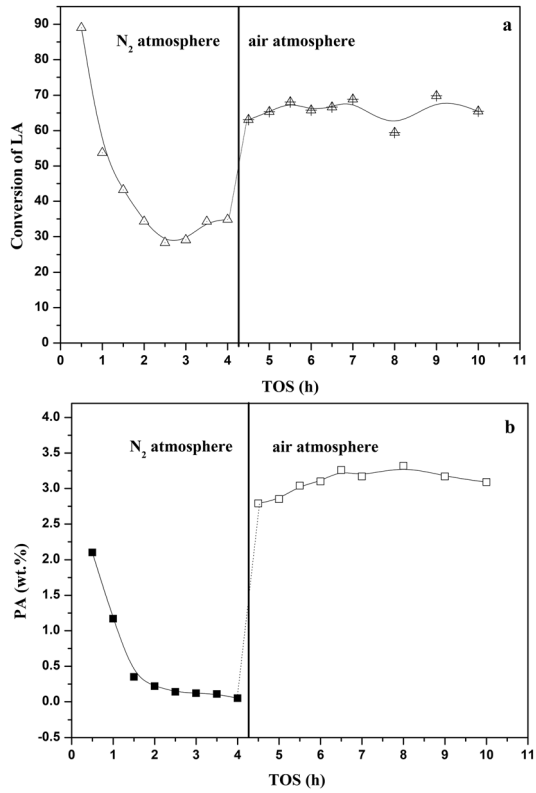

Fig. 12 Performance of the FeMoO/P catalyst at 230 °C: (a) LA conversion with time on stream, and PA concentration with time on stream (b).

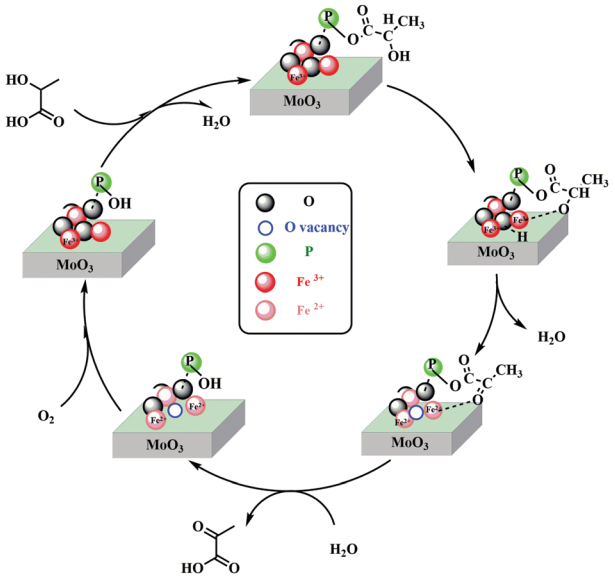

Scheme 1 Reaction mechanism for the oxidative dehydrogenation of LA to PA over the FeMoO/P catalyst.

carboxyl group (–COOH) in the LA molecule reacted with P–OH (basic site) in the catalyst to form lactate (I), accompanied with the removal of the H_2O molecule. In this step, the carboxyl group was protected. Then, the secondary alcohol was deprotonated in adsorbed lactate by Fe species to form the Fe–O intermediate (II),

and the hydride transformed to O in the adjacent Fe–O, forming Fe–OH. According to the XPS characterization of samples, the electron transfer of Fe species toward Mo leads to an increase of oxidation state, which favors the formation of the Fe–O intermediate (II). In the next step, the negative hydrogen ion in the methyl site was left and further transferred its two electrons to Fe species, which reduced the Fe center to produce a H_2O molecule, resulting in the formation of pyruvate (III). Meanwhile, pyruvate (III) adsorbed on the surface of the catalyst was hydrolysed to produce PA by acid catalysis and regenerated the basic OH group on the phosphide. The appropriate acid sites existing on the surface of the catalysts was verified by isopropanol conversion experiments, which also favors the hydrolysis of the pyruvate intermediate (III). After desorption of water, the Fe (+3) center was reduced to the +2 state. The molecular oxygen in the air oxidized the surface Fe^{2+} species back to the +3 state, and it was transformed into lattice oxygen. As a result, a catalytic cycle was completed over the FeMoO/P catalyst in the presence of oxygen.

The effect of acidity–basicity of catalysts together with their redox properties on reaction performance for LA conversion was further discussed. In the reported work,[14,20,51] the catalysts have only acidic–basicity, and not redox properties. These catalysts are used to catalyze LA conversion, and the obtained major products are acrylic acid, acetaldehyde, and 2,3-pentanedione in LA conversion *via* LA dehydration, LA decarboxylation, and LA condensation.[36,52–55] More importantly, PA is not reported as a minor side product, suggesting that the redox of the catalyst is necessary for formation of PA from LA. In addition, the catalysts combining acidic–basicity and redox properties have catalyzed LA conversion to form PA at lower reaction temperature (*ca.* 230 °C) than acidity–basicity catalyzed LA conversion alone (*ca.* >300 °C). These results indicate that controlling the lower reaction temperature is favorable for enhancing PA selectivity, and decreasing the side reactions to form acrylic acid and acetaldehyde.

Nitrogen is used as the reaction atmosphere (0–4 h on stream), and air is used as the reaction atmosphere (4.5–10 h on stream). LA, lactic acid; PA, pyruvic acid.

Experimental

Materials

L-(+)-Lactic acid (80 wt% and 98.5 wt%, fermentation type with maize) was obtained from Henan Jindan Lactic Acid Technology Co., Ltd; the former (80 wt%) was directly used for the oxidative dehydrogenation of LA to pyruvic acid without further purification, and the latter (98.5 wt%) was used as a standard reference sample. Pyruvic acid, acetaldehyde, acetone, acrylic acid, and isopropanol were purchased from Sinopharm Chemical Reagent Co., Ltd. Acetaldehyde, acetone, and acrylic acid were used for gas chromatograph reference samples, and isobutyl alcohol was used as an internal standard sample. Pyruvic acid was used for the standard reference sample in analysis with a liquid chromatograph. Ferric nitrate, ammonium phosphomolybdate and urea were purchased from Energy Chemical Company, which were used for the preparation of catalysts.

Preparation of catalysts

Fe–Mo bimetallic oxide catalysts decorated by elemental P (denoted as FeMoO/P) as well as the corresponding single metallic oxides (FeO/MoO) were synthesized by a hydrothermal method under alkaline conditions, followed by calcination in air. In a typical experiment to prepare FeMoO/P, 8 mmol of $Fe(NO_3)_3{\cdot}9H_2O$, 1.33 mmol of ammonium phosphomolybdate ($(NH_4)_3PMo_{12}O_{40}{\cdot}H_2O$) and 36 mmol of $CO(NH_2)_2$ were dissolved in 60 mL of distilled water and stirred at room temperature for 20 min. Next, the resultant solution was transferred to a 100 mL of PTFE-lined stainless steel hydrothermal reactor, placed in an oven, and kept at 120 °C for 8 h. Then, the precipitate was formed, and washed several times with distilled water and absolute ethanol, and dried at 50 °C for 3 h. Besides, the corresponding single metallic oxides, FeO and MoO, were prepared in a similar manner. Prior to their use for catalyzing the oxidative dehydrogenation of LA and catalyst characterization, all catalysts were calcined at 500 °C for 3 hours in air. In addition, the mixed catalyst (denoted as FeMoO/P*) was prepared by direct mixing using two corresponding single metallic oxides (FeO and MoO).

Catalyst characterization

The specific surface areas of catalysts were measured through nitrogen adsorption at 77 K using a JW-BK100C instrument. The pore size of catalysts is calculated from desorption branch data using the Barrett–Joyner–Halenda (BJH) model. Powder X-ray diffraction measurement was conducted on a Dmax/Ultima IV diffractometer operating at 40 kV and 20 mA with Cu-Kα radiation. The FTIR spectra of the catalysts were recorded in the range of 500–4000 cm^{-1} on a FTIR-8400S spectrometer. Diffuse reflectance UV-Vis spectra were recorded on a Shimadzu UV-2401 PC spectrometer in diffuse-reflectance mode using an integrating sphere (internal diameter 60 mm) and $BaSO_4$ was used as the reference. Redox properties of the samples were estimated by H_2-TPR on a Finesorb-3010 Instrument. X-ray photoelectron spectroscopy (XPS) measurements were performed using a Thermo Scientific K-Alpha spectrometer, equipped with a monochromatic small-spot X-ray source and a 180° double focusing hemispherical analyzer with a 128-channel detector. The binding energy was corrected for surface charging by taking the C 1s peak of contaminant carbon as a reference at 284.6 eV. Surface acidic and basic properties of the samples were estimated by NH_3-TPD and CO_2-TPD, respectively, on a Finesorb-3010 Instrument. Besides, isopropanol dehydration/dehydrogenation on the catalyst to form the corresponding propylene/acetone at a reaction temperature of 240 °C was also used to characterize the acidic–basic properties of the catalyst.

Catalyst evaluation

The vapor phase oxidative dehydrogenation of LA to pyruvic acid was performed with a continuous up-down fixed-bed quartz tubular reactor (4 mm inner diameter) under atmospheric pressure. The catalyst (*ca.* 0.35 g, 20–40 meshes) was placed between two layers of quartz wool inside the reactor. First, the catalyst was heated from room temperature to 230 °C at a rate of

3 °C min^{-1}, and kept at the temperature for 1.0 h by flowing air (3.0 mL min^{-1}). Then, the feedstock (10 wt% aqueous solution of LA, 2.0 mL h^{-1}) was pumped into the reactor and driven through the catalyst bed by air (0.1 MPa, 3.0 mL min^{-1}). The contact time of the reactant over the catalyst was estimated to be around 0.30 s according to previous ref. 44 and 56. The liquid products were analyzed off-line using an SP-6890 gas chromatograph with a FFAP capillary column connected to a FID for acrylic acid and acetaldehyde, and a LC-20AD liquid chromatograph with a reversed-phase C18 column connected to a UV detector for lactic acid and pyruvic acid.

Conclusions

The catalytic oxidative dehydrogenation of lactic acid to pyruvic acid over the FeMoO/P catalyst and its single components was investigated under various reaction conditions. It was found that pyruvic acid was formed from lactic acid *via* oxidative dehydrogenation, and not from direct dehydrogenation. FeMoO/P offered a more excellent activity than its corresponding single components and FeMoO/P* prepared by a mechanical mixing method, which was ascribed to forming the surface substituted Fe–O_x–Mo solid solution and electron transfer between Fe and Mo, leading to novel redox and acidic–basic properties that are favorable for the oxidative dehydrogenation of lactic acid. The experiments substituting nitrogen for air as a reaction atmosphere demonstrated that lattice oxygen participated in the oxidative dehydrogenation of lactic acid. Promoting adsorption of gas phase oxygen and its transformation into lattice oxygen can efficiently enhance catalytic performance, which is dependent on optimizing LA/O_2 molar ratios.

Conflicts of interest

There are no conflicts to declare.

Acknowledgements

This work was supported by the Youth/Key Project of Science and Technology Research Program of Chongqing Education Commission of China (KJZD-K201901104 and KJQN201801109), the Opening Foundation of Jiangsu Key Laboratory of Vehicle Emissions Control (OVEC 049), the Natural Science Foundation of Chongqing (cstc2019jcyj-msxmX0198), the Special Project of Technology Innovation and Application Development of Chongqing (cstc2019jscx-msxmX0002), and the Initial Scientific Research Foundation of Chongqing University of Technology (2017ZD47 and 2017ZD48).

Notes and references

1 T. D. Swift, H. Nguyen, Z. Erdman, J. S. Kruger, V. Nikolakis and D. G. Vlachos, *J. Catal.*, 2016, **333**, 149–161.
2 R. Beerthuis, G. Rothenberg and N. R. Shiju, *Green Chem.*, 2015, **17**, 1341–1361.
3 S. Suganuma, K. Nakajima, M. Kitano, D. Yamaguchi, H. Kato, S. Hayashi and M. Hara, *J. Am. Chem. Soc.*, 2008, **130**, 12787–12793.
4 B. Tabah, I. N. Pulidindi, V. R. Chitturi, L. M. R. Arava, A. Varvak, E. Foran and A. Gedanken, *J. Mater. Chem. A*, 2017, **5**, 15486–15506.
5 C. Zhang, T. Wang, X. Liu and Y. Ding, *J. Mol. Catal. A: Chem.*, 2016, **424**, 91–97.
6 G. Y. Yang, Y. H. Ke, H. F. Ren, C. L. Liu, R. Z. Yang and W. S. Dong, *Chem. Eng. J.*, 2016, **283**, 759–767.
7 M. Tao, X. Yi, I. Delidovich, R. Palkovits, J. Shi and X. Wang, *ChemSusChem*, 2015, **8**, 4195–4201.
8 L. S. Sharninghausen, B. Q. Mercado, R. H. Crabtree and N. Hazari, *Chem. Commun.*, 2015, **51**, 16201–16204.
9 F. L. Marques, A. C. Oliveira, J. Mendes, E. Rodriguez-Castellon, C. L. Cavalcante and R. S. Vieira, *Fuel Process. Technol.*, 2015, **138**, 228–235.
10 L. S. Sharninghausen, J. Campos, M. G. Manas and R. H. Crabtree, *Nat. Commun.*, 2014, **5**, 9.
11 D. Esposito and M. Antonietti, *ChemSusChem*, 2013, **6**, 989–992.
12 Y. L. Wang, W. P. Deng, B. J. Wang, Q. H. Zhang, X. Y. Wan, Z. C. Tang, Y. Wang, C. Zhu, Z. X. Cao, G. C. Wang and H. L. Wan, *Nat. Commun.*, 2013, **4**, 1–7.
13 J. Nagengast, S. Hahn, N. Taccardi, M. Kehrer, J. Kadar, D. Collias, P. Dziezok, P. Wasserscheid and J. Albert, *ChemSusChem*, 2018, **11**, 2936–2943.
14 L. L. Zhang, D. S. Theng, Y. H. Du, S. B. Xi, L. Huang, F. Gao, C. Wang, L. W. Chen and A. Borgna, *Catal. Sci. Technol.*, 2017, **7**, 6101–6111.
15 Z. B. Huo, J. F. Xiao, D. Z. Ren, F. M. Jin, T. Wang and G. D. Yao, *Green Chem.*, 2017, **19**, 1308–1314.
16 X. L. Li, J. Pang, J. Zhang, C. Y. Yin, W. X. Zou, C. M. Tang and L. Dong, *Ind. Eng. Chem. Res.*, 2019, **58**, 101–109.
17 C. Zhang, T. Wang and Y. J. Ding, *Appl. Catal., A*, 2017, **533**, 59–65.
18 K. T. Liu, X. M. Huang, E. A. Pidko and E. J. M. Hensen, *Green Chem.*, 2017, **19**, 3014–3022.
19 X. L. Li, Y. Zhang, Z. Chen, P. Can, W. X. Zou, C. M. Tang, L. Dong and Y. Wang, *Ind. Eng. Chem. Res.*, 2017, **56**, 14437–14446.
20 M. E. Sad, L. F. G. Pena, C. L. Padro and C. R. Apesteguia, *Catal. Today*, 2018, **302**, 203–209.
21 P. Maki-Arvela, I. L. Simakova, T. Salmi and D. Y. Murzin, *Chem. Rev.*, 2014, **114**, 1909–1971.
22 S. Sugiyama, T. Kikumoto, H. Tanaka, K. Nakagawa, K.-I. Sotowa, K. Maehara, Y. Himeno and W. Ninomiya, *Catal. Lett.*, 2009, **131**, 129–134.
23 T. Tsujino, S. Ohigashi, S. Sugiyama, K. Kawashiro and H. Hayashi, *J. Mol. Catal.*, 1992, **71**, 25–35.
24 S. X. Miao, L. Song, H. Li, X. B. Li, L. S. Xing and M. S. Li, *Chin. J. Inorg. Chem.*, 2014, **30**, 1325–1330.
25 M. Ai and K. Ohdan, *Appl. Catal., A*, 1997, **165**, 461–465.
26 S. Lomate, T. Bonnotte, S. Paul, F. Dumeignil and B. Katryniok, *J. Mol. Catal. A: Chem.*, 2013, **377**, 123–128.
27 M. Ai and K. Ohdan, *Chem. Lett.*, 1995, 405.

28 M. Ai, *Appl. Catal., A*, 2002, **232**, 1–6.
29 M. Ai, *Appl. Catal., A*, 2002, **234**, 235–243.
30 B. Yan, L. Z. Tao, Y. Liang and B. Q. Xu, *ACS Catal.*, 2014, **4**, 1931–1943.
31 C. M. Tang, Z. J. Zhai, X. L. Li, L. W. Sun and W. Bai, *J. Catal.*, 2015, **329**, 206–217.
32 A. L. Chen, X. J. Yu, Y. Zhou, S. Miao, Y. Li, S. Kuld, J. Sehested, J. Y. Liu, T. Aoki, S. Hong, M. F. Camellone, S. Fabris, J. Ning, C. C. Jin, C. W. Yang, A. Nefedov, C. Woll, Y. M. Wang and W. J. Shen, *Nat. Catal.*, 2019, **2**, 334–341.
33 Y. Liu, Y. X. Yu and W. D. Zhang, *Electrochim. Acta*, 2012, **59**, 121–127.
34 B. Yan, L. Z. Tao, A. Mahmood, Y. Liang and B. Q. Xu, *ACS Catal.*, 2017, **7**, 538–550.
35 X. H. Zhang, L. Lin, T. Zhang, H. O. Liu and X. F. Zhang, *Chem. Eng. J.*, 2016, **284**, 934–941.
36 G. M. Lari, B. Puertolas, M. S. Frei, C. Mondelli and J. Perez-Ramirez, *ChemCatChem*, 2016, **8**, 1507–1514.
37 C. M. Tang, J. S. Peng, X. L. Li, Z. J. Zhai, W. Bai, N. Jiang, H. J. Gao and Y. W. Liao, *Green Chem.*, 2015, **17**, 1159–1166.
38 X. L. Li, L. W. Sun, W. X. Zou, P. Cao, Z. Chen, C. M. Tang and L. Dong, *ChemCatChem*, 2017, **9**, 4621–4627.
39 J. F. Zhang, X. Z. Feng, Y. L. Zhao, W. J. Ji and C. T. Au, *J. Ind. Eng. Chem.*, 2014, **20**, 1353–1358.
40 G. C. Gunter, D. J. Miller and J. E. Jackson, *J. Catal.*, 1994, **148**, 252–260.
41 K. M. A. Santos, E. M. Albuquerque, G. Innocenti, L. E. P. Borges, C. Sievers and M. A. Fraga, *ChemCatChem*, 2019, **11**, 3054–3063.
42 S. T. Oyama, X. M. Zhang, J. Q. Lu, Y. F. Gu and T. Fujitani, *J. Catal.*, 2008, **257**, 1–4.
43 A. Sachse, V. Hulea, A. Finiels, B. Coq, F. Fajula and A. Galarneau, *J. Catal.*, 2012, **287**, 62–67.
44 Z. J. Zhai, X. L. Li, C. M. Tang, J. S. Peng, N. Jiang, W. Bai, H. J. Gao and Y. W. Liao, *Ind. Eng. Chem. Res.*, 2014, **53**, 10318–10327.
45 X. L. Li, Z. J. Zhai, C. M. Tang, L. W. Sun, Y. Zhang and W. Bai, *RSC Adv.*, 2016, **6**, 62252–62262.
46 Y. Zhang, X. Li, L. Sun and C. Tang, *ChemistrySelect*, 2016, **1**, 5002–5007.
47 H. J. Wang, D. H. Yu, P. Sun, J. Yan, Y. Wang and H. Huang, *Catal. Commun.*, 2008, **9**, 1799–1803.
48 J. H. Hong, J. M. Lee, H. Kim, Y. K. Hwang, J. S. Chang, S. B. Halligudi and Y. H. Han, *Appl. Catal., A*, 2011, **396**, 194–200.
49 M. Behrens, F. Studt, I. Kasatkin, S. Kuhl, M. Havecker, F. Abild-Pedersen, S. Zander, F. Girgsdies, P. Kurr, B. L. Kniep, M. Tovar, R. W. Fischer, J. K. Norskov and R. Schlogl, *Science*, 2012, **336**, 893–897.
50 P. Liu and E. J. M. Hensen, *J. Am. Chem. Soc.*, 2013, **135**, 14032–14035.
51 G. Näfe, M. A. López-Martínez, M. Dyballa, M. Hunger, Y. Traa, T. Hirth and E. Klemm, *J. Catal.*, 2015, **329**, 413–424.
52 Y. Matsuura, A. Onda, S. Ogo and K. Yanagisawa, *Catal. Today*, 2014, **226**, 192–197.
53 Z. Guo, D. S. Theng, K. Y. Tang, L. L. Zhang, L. Huang, A. Borgna and C. Wang, *Phys. Chem. Chem. Phys.*, 2016, **18**, 23746–23754.
54 L. W. Sun, X. L. Li and C. M. Tang, *Acta Phys.-Chim. Sin.*, 2016, **32**, 2327–2336.
55 C. M. Tang, Y. Zhang, X. L. Li, P. H. Tan, W. X. Zou, L. Dong, J. Pang and J. Zhang, *Chin. J. Inorg. Chem.*, 2019, **35**, 819–827.
56 J. F. Zhang, J. P. Lin and P. L. Cen, *Can. J. Chem. Eng.*, 2008, **86**, 1047–1053.

